BIOCHEMISTRY

 Volume 44, Number 35 September 6, 2005

Articles

Transition State Structure of 5′-Methylthioadenosine/*S*-Adenosylhomocysteine Nucleosidase from *Escherichia coli* and Its Similarity to Transition State Analogues†

Vipender Singh,‡ Jeffrey E. Lee,§ Sara Núñez,‡ P. Lynne Howell,§ and Vern L. Schramm*,‡

Department of Biochemistry, Albert Einstein College of Medicine, 1300 Morris Park Avenue, Bronx, New York 10461, and Structural Biology and Biochemistry, Research Institute, Hospital for Sick Children, 555 University Avenue, Toronto, Ontario MG5 1X8, Canada

Received May 10, 2005; Revised Manuscript Received June 24, 2005

ABSTRACT: Methylthioadenosine/*S*-adenosylhomocysteine nucleosidase (MTAN) catalyzes reactions linked to polyamine metabolism, quorum sensing pathways, methylation reactions, and adenine salvage. It is a candidate target for antimicrobial drug design. Kinetic isotope effects (KIEs) were measured on the MTAN-catalyzed hydrolysis of 5′-methylthioadenosine (MTA) to determine the transition state structure. KIEs measured at pH 7.5 were near unity due to the large forward commitment to catalysis. Intrinsic KIEs were expressed by increasing the pH to 8.5. Intrinsic KIEs from MTAs labeled at 1′-^{3}H, 1′-^{14}C, 2′-^{3}H, 4′-^{3}H, 5′-^{3}H, 9-^{15}N, and Me-^{3}H$_3$ were 1.160 ± 0.004, 1.004 ± 0.003, 1.044 ± 0.004, 1.015 ± 0.002, 1.010 ± 0.002, 1.018 ± 0.006, and 1.051 ± 0.002, respectively. The large 1′-^{3}H and small 1′-^{14}C KIEs indicate that the *Escherichia coli* MTAN reaction undergoes a dissociative (D_N*A_N) (S_N1) mechanism with little involvement of the leaving group or participation of the attacking nucleophile at the transition state, causing the transition state to have significant ribooxacarbenium ion character. A transition state constrained to match the intrinsic KIEs was located with density functional theory [B3LYP/6-31G(d,p)]. The leaving group (N9) is predicted to be 3.0 Å from the anomeric carbon. The small β-secondary 2′-^{3}H KIE of 1.044 corresponds to a modest 3′-endo conformation for ribose and a H1′−C1′−C2′−H2′ dihedral angle of 53° at the transition state. Natural bond orbital analysis of the substrate and the transition state suggests that the 4′-^{3}H KIE is due to hyperconjugation between the lone pair (n_p) of O3′ and the antibonding (σ*) orbital of the C4′−H4′ group, and the methyl-^{3}H$_3$ KIE is due to hyperconjugation between the n_p of sulfur and the σ* of methyl C−H bonds. Transition state analogues that resemble this transition state structure are powerful inhibitors, and their molecular electrostatic potential maps closely resemble that of the transition state.

Methylthioadenosine/*S*-adenosylhomocysteine nucleosidase (MTAN)[1] plays an important role in biological processes, including polyamine biosynthesis, methylation, purine salvage, and quorum sensing (*1*−*7*). It catalyzes the physiologically irreversible hydrolytic depurination of 5′-methylthioadenosine (MTA) to generate adenine and 5-methylthioribose (Figure 1a). Adenine is salvaged by adenine phosphoribosyltransferase, and the 5-methylthioribose (MTR) can be recovered in the methionine salvage pathway (*8*). In *Escherichia coli*, MTA is generated as a byproduct of

† Supported by research grants from the National Institutes of Health and the Canadian Institute for Health Research (CIHR, 43998).

* To whom correspondence should be addressed. Telephone: (718) 430-2813. Fax: (718) 430-8565. E-mail: vern@aecom.yu.edu.

‡ Albert Einstein College of Medicine.

§ Hospital for Sick Children.

10.1021/bi050863a CCC: $30.25
Published on Web 08/09/2005

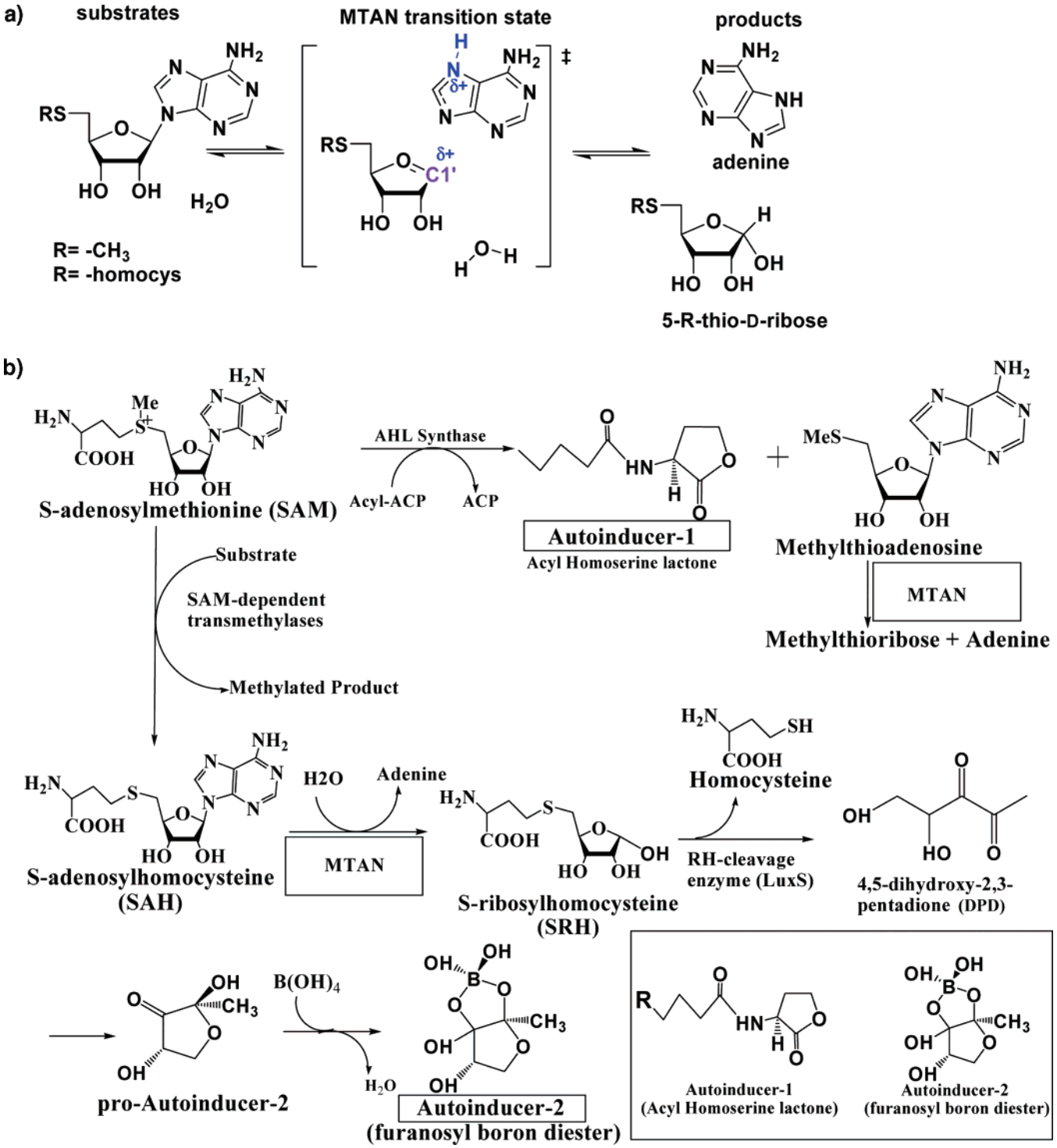

FIGURE 1: Hydrolysis of MTA by *E. coli* MTAN and the proposed transition state of the reaction (a). Features of the transition state that distinguish it from substrate are colored blue. (b) Synthesis and structures of bacterial quorum-sensing molecules, autoinducer-1 and autoinducer-2. Furanosyl-based autoinducer-2 molecules that do not contain boron have been described previously (*48*).

polyamine synthesis from the reaction involving transfer of the aminopropyl group from decarboxylated SAM to putresine. Spermidine synthase is reported to be sensitive to product inhibition by MTA with an inhibition constant of 50 μM for rat spermidine synthase (*9*). Mammalian spermine synthase is more sensitive to MTA, with a K_i value of 0.3 μM (*10*). Inhibition of MTAN is therefore expected to inhibit polyamine biosynthesis and the salvage pathways for adenine and methionine. In bacteria, MTA is also produced as a byproduct in the synthesis of acyl homoserine lactones (AHL) from *S*-adenosylmethionine (SAM) and acyl-ACP in a reaction catalyzed by AHL synthase (*11*). Acylhomoserine lactones are also known as autoinducers-1 (AI1) and are used by Gram-negative bacteria for quorum sensing (Figure 1b). MTA has an inhibitory effect on AHL synthase (50 μM produces 67% inhibition) (*11*). In addition to MTA, MTAN also catalyzes hydrolysis of *S*-adenosylhomocysteine (SAH) to generate adenine and *S*-ribosylhomocysteine (SRH). SRH is subsequently converted to a group of furanone-like molecules that are collectively known as autoinducer-2 (AI2)

(one example is shown in Figure 1b) (*12*). Autoinducers (AI1 and AI2) mediate quorum sensing in bacteria to regulate processes such as biofilm formation, virulence, and antibiotic resistance. Disruption of these pathways by inhibiting MTAN presents a potential target for interfering with biofilm formation and autoinducer-mediated antibiotic resistance pathways.

Transition state theory predicts that enzymes catalyze reactions by lowering the activation barrier, and the catalytic acceleration imposed by the enzyme is proportional to the enzymatic stabilization of the transition state (*13*, *14*). Transition state analogue inhibitors are designed from the hypothesis that chemically stable analogues that mimic geometric and molecular electrostatic features of the transition state will bind to the enzyme tighter than the substrate by a factor approaching the catalytic rate acceleration imposed by the enzyme. For nucleoside hydrolases, the calculation predicts a binding affinity of $10^{-19}-10^{-18}$ M for mimics of the transition state (*15*−*17*). However, it is not possible to design "perfect" transition state analogues since the actual enzymatic transition state involves nonequilibrium bond lengths and charges that cannot be accurately copied to chemically stable molecules.

Kinetic isotope effects (KIEs) using isotopically labeled substrates combined with computational chemistry are the preferred method for understanding the transition states of enzymatic reactions (*18*−*21*). KIEs are defined as the ratio of reaction rates for normal and isotopically labeled substrate. Competitive KIEs measure the effect on k_{cat}/K_m which includes all steps from free reactants to the first irreversible step of the reaction. Intrinsic isotope effects occur when the first irreversible step is bond breaking at the transition state and none of the intervening steps present a significant energetic barrier. Intrinsic KIEs report the difference between bond vibrational ground states for the reactants free in solution and at the transition state. Computational modeling of transition states is facilitated by using intrinsic KIEs as experimental boundary conditions.

Kinetic isotope effects have been used to study the transition states of *N*-ribosyltransferases, including nucleoside hydrolase, purine nucleosidase phosphorylase (PNP), ricin-A chain, and thymidine phosphorylase (*16*, *18*−*20*). Most *N*-ribosyltransferases (with the exception of thymidine phosphorylase) have dissociative S_N1 reaction mechanisms with transition states exhibiting ribooxacarbenium ion character. Transition state analogue inhibitors have been designed for some of these enzymes by incorporating properties of their transition states into chemically stable analogues. They are powerful inhibitors. One such example is Immucillin-H,[2] a transition state analogue inhibitor of human and bovine PNPs that binds with dissociation constants of 56 and 23 pM, respectively. It is currently in clinical trials for T-cell leukemia under the name Fodosine.[3] Second-generation transition state analogues designed specifically to match the transition state of human PNP are tight-binding inhibitors with K_d values of 7 pM, and one of these is in clinical trials for psoriasis (*22*).[3]

In this study, we investigated the transition state of *E. coli* MTAN using multiple KIEs and obtained its geometric and electrostatic properties using density functional methods. We found that the *E. coli* MTAN has a dissociative transition state with significant oxacarbenium ion character. Natural bond orbital (NBO) analysis of the substrate and the transition state was used to help understand the observed isotope effects. The transition state structure of *E. coli* MTAN obtained here predicted that transition state analogue inhibitors resembling MTA with riboxacarbenium features in the ribosyl group and elevated pK_a values in the leaving group adenine analogue would be powerful inhibitors. These analogues resemble those previously described for 5′-methylthioadenosine phosphorylase and with MTAN, and have dissociation constants that extend into the femtomolar range (*23*).

MATERIALS AND METHODS

Enzyme Preparation. MTAN from *E. coli* was obtained as described previously (*17*, *24*). The histidine tag was removed by chymotrypsin digestion following purification. The digested protein consists of 232 amino acids belonging to *E. coli* MTAN and 10 residues from the N-terminal histidine fusion tag. The protein was analyzed for purity in SDS−PAGE gels stained with Coomassie blue and was stored at 15 mg/mL at −70 °C following flash-freezing in dry ice and acetone.

Enzymes and Reagents for MTA Synthesis. Hexokinase, myokinase, pyruvate kinase, glucose-6-phosphate dehydrogenase, phosphoriboisomerase, and phosphogluconic dehydrogenase were purchased from Sigma. Adenine phosphoribosyltransferase from yeast (APRTase) was reported previously (*25*); 5′-phosphoribosylpyrophosphate synthetase (PRPPase) was a gift from P. Berti (McMaster University, Hamilton, ON), and SAM synthetase was provided by G. D. Markham (Fox Chase Cancer Center, Philadelphia, PA). ATP, monopotassium α-ketoglutarate, glucose, β-nicotinamide adenine dinucleotide phosphate sodium salt ($NADP^+$), phosphoenolpyruvic acid cyclohexylammonium salt (PEP), glycylglycine, and dithiothreitol (DTT) were purchased from Sigma.

Synthesis of Radiolabeled ATPs. [1′-^{3}H]ATP, [1′-^{14}C]ATP, [5′-^{14}C]ATP, [5′-^{3}H]ATP, and [4′-^{3}H]ATP were synthesized enzymatically from [1-^{3}H]ribose, [2-^{14}C]glucose, [6-^{14}C]-glucose, [6-^{3}H]glucose, and [5-^{3}H]glucose, respectively (purchased from American Radiochemicals Inc.), as shown in Figure 2a (*26*). [2′-^{3}H]ATP was synthesized from [2-^{3}H]-ribose 5-phosphate as described previously (*27*). [9-^{15}N,5′-^{14}C]ATP was synthesized from [9-^{15}N]adenine and [6-^{14}C]-glucose. The reaction mixture for the synthesis of radiolabeled ATPs from glucose contained 100 mM phosphate buffer (pH

[1] Abbreviations: MTA, 5′-methylthioadenosine; SAH, *S*-adenosylhomocysteine; SAM, 5-adenosylmethionine; MTR, 5-methylthioribose; MTAN, 5′-methylthioadenosine/*S*-adenosylhomocysteine nucleosidase; MT-ImmA and MT-Immucillin-A, (1*S*)-1-(9-deazaadenin-9-yl)-1,4-dideoxy-1,4-imino-5-methylthio-D-ribitol; *p*ClPhT-ImmA, (1*S*)-5-(4-chlorophenylthio)-1-(9-deazaadenin-9-yl)-1,4-dideoxy-1,4-imino-D-ribitol; MT-DADMe-ImmA and 5′-methylthio-DADMe-Immucillin-A, (3*R*,4*S*)-1-[(9-deazaadenin-9-yl)methyl]-3-hydroxy-4-(methylthiomethyl)pyrrolidine; *p*ClPhT-DADMe-ImmA, (3*R*,4*S*)-4-(4-chlorophenylthiomethyl)-1-[(9-deazaadenin-9-yl)methyl]-3-hydroxypyrrolidine.

[2] Immucillin-H is (1*S*)-1-(9-deazahypoxanthin-9-yl)-1,4-dideoxy-1,4-imino-D-ribitol and has been shown to have a pK_a of 6.9 at N4′ and of >10 at N7 (*44*). MT-ImmA is chemically similar in the 9-deazaadenine ring and is expected to have a similar pK_a.

[3] See http://www.biocryst.com for clinical trial information.

7.5), 50 mM glycylglycine (pH 8.0), 50 mM KCl, 20 mM $MgCl_2$, 1 mM glucose, 40 mM PEP, 20 mM α-ketoglutarate, 1 mM DTT, 0.1 mM $NADP^+$, 10 mM adenine, and 10−50 μCi of labeled D-glucose in a reaction volume of 1 mL. To the reaction mixture were added 4.0 units of myokinase, 3.0 units of pyruvate kinase, 5.0 units of phosphoriboisomerase, 1.0 unit of glucose-6-phosphate dehydrogenase and phosphogluconic acid dehydrogenase, and 5 units of APRTase and PRPPase. The synthesis was initiated by adding 0.1 unit of hexokinase. Reaction mixtures were incubated for 12 h at 37 °C, and the ATP was purified by reverse phase HPLC on a Waters C-18 Deltapak column using a methanol, ammonium acetate, and water solvent with overall yields in the range of 50−80%. Following purification, the compounds were freeze-dried, dissolved in water, and stored at −80 °C.

Synthesis of Radiolabeled MTAs. [1′-^{3}H]MTA, [1′-^{14}C]-MTA, [2′-^{3}H]MTA, [3′-^{3}H]MTA, [4′-^{3}H]MTA, [5′-^{3}H]MTA, and [2, 8-^{3}H]MTA were synthesized from the corresponding ATP molecules in two steps (Figure 2b). In the first step, ATP was converted to SAM in a 1 mL reaction mixture containing 100 mM Tris (pH 7.9), 50 mM KCl, 20 mM $MgCl_2$, 7% β-mercaptoethanol, 10 mM methionine, 1 unit of inorganic pyrophosphatase, and ∼0.1 unit of SAM synthetase. The reactions were completed in 4 h in 90−95% yield. SAM was subsequently converted to MTA by acid hydrolysis at 75 °C. This reaction is pH sensitive, and the maximum yield was obtained at pH 3−4, obtained by adding 100 μL of 1 M citrate buffer (pH 3.0) to the reaction mixture. SAM was converted to MTA with an ∼80% yield in 3.5 h. MTA was purified by reverse phase HPLC first using 10% methanol (by volume) in 100 mM triethylammonium acetate (pH 5.0) as the solvent and then in a second step using 50% methanol (by volume) in water as the solvent. Purified MTAs were lyophilized and stored at −70 °C in 50% ethanol.

Kinetic Isotope Effect Measurements. Competitive kinetic isotope effects (KIEs) for isotopic substitutions at various positions on the substrate were measured by comparing the relative rate of product formation from pairs of isotopically labeled substrates. Reaction mixtures contained a mixture of ^{3}H- and ^{14}C-labeled substrates with a 4:1 ^{3}H:^{14}C ratio. The MTAN assay was performed in triplicates of 1 mL reaction mixtures [100 mM HEPES (pH 7.5−8.5), 50 mM KCl, 250 μM MTA (including label), and 0.5−1 nM MTAN] containing $>10^5$ cpm of ^{14}C. After 20−30% completion of the reaction, 750 μL of the reaction was resolved on charcoal−Sepharose (acid-washed powdered charcoal and Sepharose in a 1:4 ratio made into a slurry in 1 mM MTR and settled in Pasteur pipets). The remainder of the reaction mixture was allowed to react to completion and then applied to the column. Columns were washed with 2 volumes of 1 mM MTR, and radioactive methylthioribose was eluted with 6 volumes of 15 mM MTR containing 50% ethanol. Each 1.0 mL of eluate was mixed with 9.0 mL of scintillation fluid and counted for at least three cycles at 10 min per cycle. The ^{3}H:^{14}C ratio was determined for partial and complete reactions, and the KIEs were corrected to 0% hydrolysis by the equation

$$\mathrm{KIE} = \frac{\ln(1-f)}{\ln\left(1 - f\frac{R_f}{R_o}\right)}$$

where f is the fraction of reaction progress and R_f and R_o are ratios of heavy to light isotope at the partial and total completion of reaction, respectively.

Commitment to Catalysis. Forward commitment to catalysis refers to partitioning of the Michaelis complex to product relative to being released unchanged into the solution (k_{cat}/k_{off}) (*28*). It was measured by isotope trapping (*29*) using rapid-mix pre-steady state conditions. Enzyme (13 μL of a 20 μM solution) in 100 mM HEPES (pH 8.5) and 50 mM KCl was mixed with an equal volume containing 200 μM [8-^{14}C]MTA in the same buffer. After 19 ms, the mixture (the pulse solution) was diluted with 975 μL of a solution containing 3 mM unlabeled MTA in 100 mM HEPES (pH 8.5) and 50 mM KCl (the chase solution). Samples (100 μL) were quenched with 1 N HCl at the indicated time and quantitated for product formation [reverse phase HPLC using a C-18 Deltapak column with 25% methanol and 50% 100 mM ammonium acetate (pH 5.0)] by scintillation counting. The forward commitment to catalysis is the fraction of bound MTA converted to product following dilution in excess MTA.

Determination of the Transition State Using Hybrid Density Functional Theory (DFT). A transition state structure that reproduced the intrinsic KIE values for the hydrolysis of MTA by *E. coli* MTAN was determined in vacuo by hybrid density functional theory implemented in *Gaussian03* (*30*) using 5′-methylthioadenosine as the substrate. The substrate and the model transition state were optimized using the three-parameter Becke (B3) exchange functional, the LYP correlation functional, and the standard 6-31G(d,p) basis set. Bond frequencies were computed for optimized structures at the same level of theory with the same basis set (*31*). The methylthio group of MTA was frozen in the substrate and the transition state by constraining the O4′−C4′−C5′−S dihedral angle to 173.5° and 166°, respectively. These dihedral angles were obtained from the crystal structure of 5′-methylthiotubericidin (MTT, a substrate analogue) and of MT-DADMe-ImmA (a transition state analogue inhibitor) with *E. coli* MTAN (*32*).

Kinetic isotope effects were calculated at 298 K from the computed frequencies with *Isoeff 98* on the basis of equations described previously (*33*). The transition state was optimized iteratively with additional constraints until the isotope effects calculated for the transition state matched the experimental intrinsic KIEs. The constraints were released prior to frequency calculations. The natural bond orbital (NBO) analysis was performed on the optimized structures by using the POP=NBO option in *Gaussian03*.

Calculations of Molecular Electrostatic Potential Surfaces. Molecular electrostatic potential (MEP) surfaces were calculated by the CUBE subprogram of *Gaussian03*. The formatted checkpoint files used in the CUBE subprogram were generated by geometry optimization at the B3LYP level of theory and with the 6-31G(d,p) basis set. The MEP surfaces were visualized using Molekel 4.0 (*34*) at a density of 0.008 electron/b (*35*).

RESULTS AND DISCUSSION

Effect of pH on Kinetic Isotope Effects. E. coli MTAN catalyzes the physiologically irreversible *N*-ribosyl hydrolysis of 5′-methylthioadenosine to adenine and 5-methylthioribose

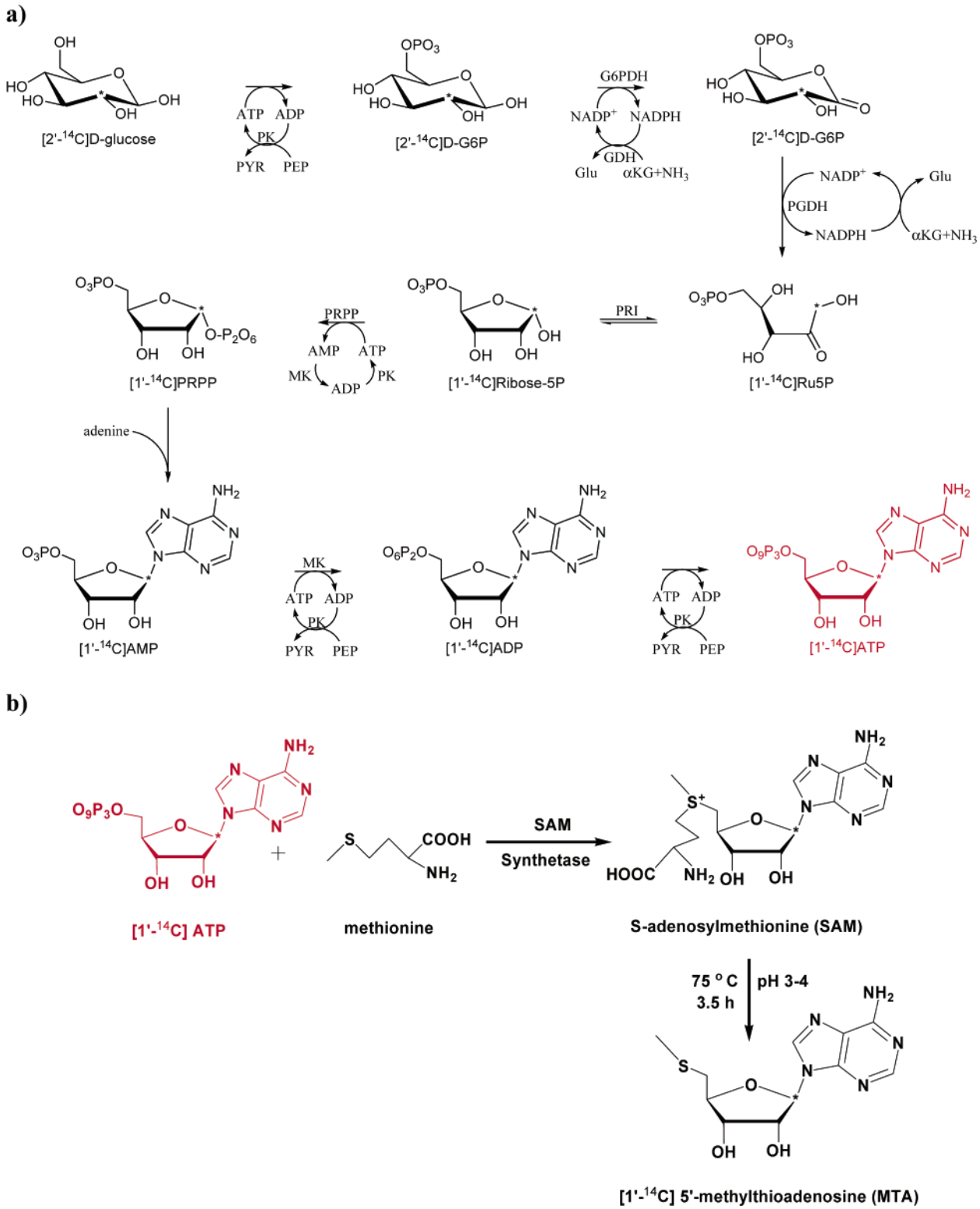

FIGURE 2: (a) Synthetic route for production of radiolabeled ATP from labeled glucose (adapted from ref *18*). This figure uses [1′-^{14}C]ATP as the example and indicates the position of the ^{14}C label with an asterisk. Details are described in Materials and Methods. (b) Synthetic route for production of radiolabeled MTA from labeled ATP. For details, see Materials and Methods.

with a k_{cat} of 20 s^{-1} at pH 7.5. The kinetic isotope effects measured at pH 7.5 were all near unity. This pattern is consistent with the suppression of isotope effects by kinetic factors and is a common problem in the determination of enzymatic transition states from KIEs (*28*, *36*, *37*). Suppression of KIEs due to large forward commitment is expected with tight-binding substrates, and the K_m for MTA of 0.43 μM suggested this to be the mode of KIE suppression. KIEs can also be suppressed by reverse commitments in chemically reversible reactions, but the hydrolytic MTAN reaction is irreversible under the conditions used here; thus, reverse commitment is considered unlikely. Forward commitment was reduced by varying the pH used in the KIE measurements. The KIE for [1′-^{3}H]MTA increased from 1.020 to

1.160 as the pH was increased from 5.5 to 8.5 but was not further altered by going to pH 9.5, suggesting that the KIE at pH 8.5 is approaching intrinsic values. The KIEs for other positions were subsequently measured at pH 8.5. At pH 8.5, the k_{cat} is reduced 14-fold and the K_m is increased to 2.0 ± 0.5 μM. An elevated pH decreases k_{cat}/K_m by a factor of 65, consistent with a change from near-full to near-zero commitment.

Commitment Correction and Intrinsic KIEs. Competitive KIEs measured experimentally give the apparent isotope effect on k_{cat}/K_m, which includes contributions from the nonchemical steps. Intrinsic isotope effects are obtained from the apparent isotope effects after they are corrected for the forward and reverse commitment using the expression derived by Northorp (*37*):

$$^{T}(V/K) = \frac{^{T}k + C_f + C_r\,^{T}K_{eq}}{1 + C_f + C_r}$$

where $^{T}(V/K)$ is an observed tritium isotope effect, C_f is the forward commitment to catalysis, C_r is the reverse commitment to catalysis, $^{T}K_{eq}$ is the equilibrium isotope effect, and ^{T}k is the intrinsic isotope effect. The hydrolytic reaction catalyzed by *E. coli* MTAN is irreversible under initial rate conditions; therefore, the above expression can be reduced to

$$^{T}(V/K) = \frac{^{T}k + C_f}{1 + C_f}$$

Forward commitment measures the effective partitioning of the Michaelis complex to product relative to being released as unchanged substrate (k_{cat}/k_{off}). It was measured at pH 8.5 using the isotope trapping method as developed by Rose et al. (*29*). The external forward commitment factor of 0.020 ± 0.027 for *E. coli* MTAN establishes that binding of MTA at pH 8.5 is freely reversible, and the isotope effects are within experimental error of their intrinsic values (Figure 3). Thermodynamically, it suggests that at pH 8.5 the ΔG barrier for the binding of the substrate to the enzyme is small relative to the ΔG for the chemical step. The $^{T}K_{eq}$ for the MTAN reaction is assumed to be near unity since the anomeric carbon is sp^3-hybridized in both the reactant and product. Thus, the experimental KIEs at pH 8.5 are within experimental error of intrinsic values (Table 1).

Correction to Remote Label KIEs. The isotope effect at 5′-^{14}C was assumed to be unity because it is three bonds distant from the reaction center and ^{14}C does not report isotope effects for geometric changes, unlike remote tritium labels (*38*−*40*). For measuring 1′-^{14}C and 9-^{15}N KIEs, [5′-^{3}H]MTA was used as the remote label. The 1′-^{14}C and 9-^{15}N KIEs were corrected for the remote label KIE. The isotope effects at 4′-^{3}H and 5′-^{3}H were significant, even though these atoms are three and four bonds, respectively, from the reaction center. Remote isotope effects have been observed for isotopic substitution at these positions in other *N*-ribosyltransferases; for example, in bovine PNP, remote isotope effects of 1.024 and 1.06 have been observed for [4′-^{3}H]- and [5′-^{3}H]inosine, respectively. The 4′-^{3}H and 5′-^{3}H KIEs for *E. coli* MTAN were smaller, 1.015 and 1.010, respectively (Table 1).

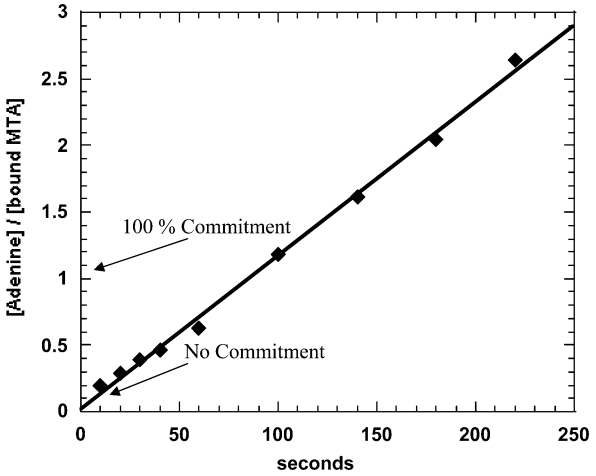

FIGURE 3: Commitment to catalysis for the MTAN−MTA complex at pH 8.5. The complex of MTAN and [^{14}C]MTA was diluted with a large excess of unlabeled MTA at 19 ms. Subsequent reaction partitions bound [^{14}C]MTA to product (forward commitment) or permits release into free, unbound MTA. Zero commitment extrapolates through the origin, while full (100%) commitment would intersect at 1.0 on the ordinate as indicated by the arrow. The forward commitment was calculated by plotting the amount of labeled adenine formed following addition of chase solution divided by the amount of labeled MTA on the active site before dilution with chase solution and extrapolating this ratio back to zero time. The line is drawn from an ordinary least-squares fit of the data, with *y* errors only. The intercept value is 0.020 ± 0.027.

Table 1: Kinetic Isotope Effects Measured at pH 8.5 for Hydrolysis of MTA by *E. coli* MTAN

substrate	type of KIE	intrinsic KIE[a]
[1′-^{3}H]- and [5′-^{14}C]MTA	α-secondary	1.160 ± 0.004
[1′-^{14}C]- and [5′-^{3}H]MTA	primary	0.994 ± 0.004
		1.004 ± 0.003[b]
[2′-^{3}H]- and [5′-^{14}C]MTA	β-secondary	1.044 ± 0.004
[9-^{15}N,5′-^{14}C]- and [5-^{3}H]MTA	primary	1.008 ± 0.002
		1.018 ± 0.006[c]
[4′-^{3}H]- and [5′-^{14}C]MTA	γ-secondary	1.015 ± 0.002
[5′-^{3}H]- and [5′-^{14}C]MTA	δ-secondary	1.010 ± 0.002
[Me-^{3}H]- and [5′-^{14}C]MTA	remote	1.051 ± 0.002

[a] KIEs are corrected to 0% substrate depletion. Since commitment factors are small (Figure 3), observed values are intrinsic KIEs except for the 1′-^{14}C and 9-^{15}N primary effects. [b] The 1′-^{14}C KIE was corrected for the 5′-^{3}H KIE according to the expression KIE = $KIE_{observed}$ × 5′-^{3}H KIE. [c] The 9-^{15}N KIE was corrected for the 5′-^{3}H KIE according to the expression KIE = $KIE_{observed}$ × 5′-^{3}H KIE.

Computational Modeling of the Transition State of E. coli MTAN. The intrinsic KIEs provide boundary conditions for the computational modeling of the transition state of *E. coli* MTAN. The 9-^{15}N KIE of 1.018 along with the 1′-^{3}H KIE of 1.160 suggests that the transition state has a small bond order to the leaving group and little participation of the attacking nucleophile. The water nucleophile was therefore not included in the calculation of the transition state. The transition state was modeled using the B3LYP level of theory and the 6-31G(d,p) basis set. The methylthio group of MTA is far from the site of nucleophilic substitution, and its conformation does not influence the magnitude of primary and secondary KIEs near C1′ and has no influence on the chemistry or conformation of the oxacarbenium ion or the leaving group. Therefore, during calculations aimed at locating the transition state, the methylthio group was constrained using the dihedral angle from the crystal structure

Table 2: Geometric and Electronic Changes in Conversion of the Substrate (GS) to the Transition State (TS) for *E. coli* MTAN [B3LYP/6-31G(d,p)]

	bond length		bond order change[a]	hyperconjugation (kcal/mol)[b] substrate		TS			orbital changes[c]			
bond type	GS	TS	$\Delta(\sigma-\sigma^*)$	$\sigma\rightarrow$	$\rightarrow\sigma^*$	$\sigma\rightarrow$	$\rightarrow\sigma^*$	$\Delta\sum$(TS−GS)	GS hybrid	carbon content (%)	TS hybrid	carbon content (%)
C1′−H1′	1.0935	1.0864	−0.01501	9.05	8.61	8.16	8.22	−1.28	$sp^{2.75}$	63.33	$sp^{1.81}$	64.13
C2′−H2′	1.0934	1.0960	0.00216	4.84	12.56	7.93[d]	9.36	−0.11	$sp^{2.56}$	63.53	$sp^{2.40}$	65.30
C4′−H4′	1.0984	1.0927	−0.00865	8.85	12.50[e]	10.06	6.74[f]	3.60	$sp^{3.02}$	62.15	$sp^{3.00}$	64.65
C1′−N9	1.4627	3.0000		7.35	26.36				$sp^{3.26}$	35.80		
C5′−H5′(*R*)	1.0940	1.0947	0.00429	4.88	4.43	3.87	7.29[g]	1.85	$sp^{3.07}$	63.50	$sp^{2.87}$	63.92
C5′−H5′(*S*)	1.0942	1.0921	−0.00246	3.78	5.33[h]	4.21	4.60	−0.30	$sp^{2.93}$	63.53	$sp^{2.78}$	64.16
C^S−H(A)	1.0919	1.0915	0.00254	2.41	1.14	0.75	3.98[i]	1.18	$sp^{2.96}$	63.13	$sp^{2.75}$	63.18
C^S−H(B)	1.0927	1.0913	−0.00113	0.00	3.99	0.00	4.00[i]	0.01	$sp^{2.82}$	62.79	$sp^{2.75}$	63.24
C^S−H(C)	1.0914	1.0915	−0.00226	0.68	4.69[j]	2.53	1.03	−1.81	$sp^{2.76}$	62.69	$sp^{2.92}$	63.88
C3′−H3′	1.0978	1.0934	−0.01269	7.46	2.26	4.06	6.95[k]	1.29	$sp^{2.78}$	62.87	$sp^{2.64}$	63.95

[a] Calculated by subtracting the number of electrons occupying the σ^* orbital from the number occupying the σ orbital and listed as the change between the substrate and transition state (TS) (substrate − TS). [b] Sum of second-order perturbation contributions calculated by NBO analysis with a cutoff of 0.5 kcal/mol. Lp1 is the sp-type lone pair, and Lp2 is a p-type lone pair. [c] Hybridization of the carbon atom and contribution of the carbon atom to the bond as a percent of bond contribution. [d] Lp2(C1′) is a better acceptor in the transition state. [e] Lp2(O4′) is a better acceptor in the substrate. [f] Lp1(O3′) is a better acceptor in the transition state. [g] Lp2(S) is a better acceptor in the transition state. [h] Lp2(S) is a better acceptor in the substrate. [i] Lp2(S) is a better acceptor in the transition state. [j] Lp2(S) is a better acceptor in the substrate. [k] Lp2(O3′) is a better acceptor in the transition state.

of *E. coli* MTAN with a transition state analogue (MT-DADMe-ImmA), a close approximation of its transition state conformation (*23*, *32*). The applied constraints on the transition state structure were iteratively optimized until the calculated KIEs closely matched the experimental KIEs. Properties of the transition state are discussed below together with a discussion of individual isotope effects.

The transition state refers to a saddle point on a potential energy surface that is characterized by a single imaginary frequency ($\nu^{\ddagger}$) in which one of the restoring vibrational modes is converted to a translation mode along the reaction coordinate (the imaginary $\nu^{\ddagger}$). The initial ab initio transition state had an imaginary frequency of 397 i cm^{-1}. However, when the transition state geometry was constrained to fit the intrinsic KIEs, two additional imaginary frequencies of approximately 178 and 54 i cm^{-1} were obtained for the transition state.[4] The smaller negative frequency of 54 i cm^{-1} corresponds to motion along the reaction coordinate, whereas the larger negative frequency of 178 i cm^{-1} arises due to constraints applied to the 5′ end of MTA. This frequency (178 i cm^{-1}) does not affect the KIEs at the reaction center, as confirmed by additional computed equilibrium isotope effects (EIEs) on the closely related intermediate structure. The transition state of *E. coli* MTAN is the in vacuo model for which the calculated KIEs match the experimental KIEs. The properties of the transition state are listed in Table 2 and are discussed in the context of individual kinetic isotope effects.

1′-^{14}C Isotope Effects. The α-primary 1′-^{14}C KIE is useful in determining the mechanism of nucleophilic substitution reactions (S_N1 vs S_N2) and is sensitive to the motion along the reaction coordinate. For a fully dissociative S_N1 transition state, the 1′-^{14}C KIE is close to unity. For a slightly associative S_N1 transition state, it is in the range of 1.01−1.03, and it is 1.080−1.13 for associative S_N2 transition states (*36*). Many *N*-ribosyltransferases have a 1′-^{14}C KIE between 1.00 and 1.03 and thus have dissociative S_N1 mechanisms with significant ribooxacarbenium character. An exception is the arsenolysis reaction of thymidine phosphorylase which has a 1′-^{14}C KIE of 1.13, implying an associative S_N2 mechanism and a neutral transition state (*20*). The primary 1′-^{14}C isotope effect of 1.004 for *E. coli* MTAN suggests a dissociative $D_N{*}A_N$ mechanism, like those of other *N*-ribosyltransferases, with the transition state exhibiting significant cationic character with low Pauling bond order to the leaving group and insignificant bond order to the attacking nucleophile. The small primary 1′-^{14}C KIE is consistent with a change in hybridization at the anomeric carbon as it changes from sp^3-hybridized carbon in the substrate to an sp^2-hybridized planar configuration of a fully dissociative transition state. The 1′-^{14}C KIE of 1.004 together with the 9-^{15}N KIE of 1.018 suggests that at the transition state anomeric carbon has minimal bond order to the adenine leaving group (N9). The transition state consistent with the intrinsic KIEs predicted N9 to be 3.0 Å from the anomeric carbon (C1′). The nucleophile was found to be >3.5 Å from the anomeric carbon since including it at this distance altered the calculated KIE beyond the errors of the experimental KIEs. The natural bond orbital analysis of the transition state and the substrate reveals that the anomeric carbon is $sp^{2.30}$-hybridized at the transition state relative to $sp^{2.83}$ in the substrate (Table 2). These changes cause increased cationic character at the transition state (positive charge on O4′ and C1′ increases by 0.20 and 0.25, respectively) relative to the reactant state. This sharing of charge is characteristic of ribooxacarbenium ions (*36*). The change in hybridization creates a partially empty $2p_z$ orbital on the anomeric carbon that hyperconjugates with the C2′−H2′ group and stabilizes the transition state by partially neutralizing the positive charge on the anomeric carbon.

1′-^{3}H Isotope Effects. A large 1′-^{3}H KIE α-secondary hydrogen kinetic isotope effect is indicative of a dissociative S_N1 transition state with oxacarbenium character, whereas a

[4] The enzymatic transition state is obtained by matching the calculated KIEs to intrinsic KIEs. In calculations for dissociative S_N1 transition states, multiple negative frequencies appear when constraints are applied to in vacuo ab initio transition states to match experimental KIEs.

Table 3: Comparison of Intrinsic KIEs for *E. coli* MTAN with Other *N*-Ribosyltransferases

		intrinsic KIEs				
position	type of KIE	*E. coli* MTAN	RNA ricin-A chain[a]	bovine PNP[b]	human PNP[c]	P.f. PNP[c]
1′-^{3}H	α-secondary	1.160 ± 0.004	1.163 ± 0.009	1.141 ± 0.004	1.184 ± 0.004	1.116 ± 0.007
1′-^{14}C	primary	1.004 ± 0.003	0.993 ± 0.004	1.026 ± 0.006	1.002 ± 0.006	0.996 ± 0.006
2′-^{3}H	*β*-secondary	1.044 ± 0.004	1.012 ± 0.004	1.152 ± 0.003	1.031 ± 0.004	1.036 ± 0.003
9-^{15}N	primary	1.018 ± 0.006	1.012 ± 0.004	1.010 ± 0.005	1.029 ± 0.006	1.019 ± 0.005
4′-^{3}H	*γ*-secondary	1.015 ± 0.002	0.992 ± 0.004	1.008 ± 0.004	1.024 ± 0.003	1.009 ± 0.002
5′-^{3}H	*δ*-secondary	1.010 ± 0.002	0.996 ± 0.003	1.033 ± 0.005	1.062 ± 0.002	1.064 ± 0.003
Me-^{3}H	remote	1.051 ± 0.002	NA	NA	NA	NA

[a] Taken from ref *19*. [b] Taken from ref *47*. [c] Taken from ref *18*. P.f. refers to *P. falciparum* PNP.

small 1′-^{3}H KIE indicates a neutral S_N2 transition state with significant participation of the nucleophile (*36*, *41*). The intrinsic 1′-^{3}H KIE of 1.16 measured for *E. coli* MTAN is consistent with a dissociative transition state with oxacarbenium ion character. The magnitude of the 1′-^{3}H KIE contains contributions from two competing factors, the out-of-plane bending mode of the C1′−H1′ group due to increased steric freedom at the transition state relative to substrate and a decrease in the "vibrational looseness" of the C1′−H1′ stretching mode at the transition state. The predominant contribution to the observed normal KIE comes from the increased out-of-plane bending motion of the C1′−H1′ *σ* bond due to reduced steric crowding at the transition state relative to substrate (*41*). The normal isotope effect caused by increased out-of-plane bending motion is opposed by the decrease in the stretching mode for the C1′−H1′ group due to the change in hybridization of the anomeric carbon from $sp^{2.83}$ in the substrate to $sp^{2.3}$ at the transition state or the increased s-character at the transition state (Table 2). The increased s-character of the anomeric carbon in the C1′−H1′ *σ* bond opposes the observed normal KIE. Although both factors contribute to the magnitude of this KIE, the relative variation in the observed 1′-^{3}H KIE for different enzymes is dominated by variation in the out-of-plane bending motion at the transition state. This mode is highly sensitive to the C1′−N9 distance and to nucleophilic participation (distance) at the transition state. The contribution of out-of-plane bending modes to the intrinsic 1′-^{3}H KIE outweighs the stretching effects, which are less sensitive to atomic distances in the reaction coordinate.

Many *N*-ribosyltransferases have S_N1 transition states that are characterized by large 1′-^{3}H KIEs. Human and *Plasmodium falciparum* PNPs both demonstrate well-developed ribooxacarbenium ions at the transition state and have 1′-^{3}H KIEs of 1.184 and 1.116, respectively, with inosine as the substrate (Table 3) (*18*). Ricin A-chain with a stem−loop RNA substrate also has a carbocation ribosyl transition state characterized by an intrinsic 1′-^{3}H KIE of 1.163 (*19*). The computational modeling of the 1′-^{3}H KIE to obtain an exact match with experimental values is difficult because of ill-defined differences between in vacuo calculations and unknown protein atomic distances at the transition state. The computed isotope effect for 1′-^{3}H MTA for the *E. coli* MTAN transition state at 298 K in a vacuum using the B3LYP/6-31G(d,p) level of theory is 1.38, more than double the measured intrinsic 1′-^{3}H KIE of 1.160. Catalytic site interactions at the transition state are proposed to dampen the out-of-plane bending motions of C−H bonds causing suppression of their intrinsic KIEs. These effects are not reproduced in the in vacuo calculations. This effect is well-known for α-secondary isotope effects (*41*), and the structure of the transition state does not depend on the matching of this value. Although the large 1′-^{3}H KIE is consistent with a ribooxacarbenium ion at the transition state, the disagreement with in vacuo ab initio calculations tells us that the transition state is a relatively crowded environment compared to vacuum. We also know this from structural studies with transition state analogues, but these lack information about the dynamic excursions of the transition state (*21*). The relatively suppressed 1′-^{3}H KIE observed here suggests a dynamically constrained environment during the short time ($\sim 10^{-13}$ s) the reactant spends at the transition state.

2′-^{3}H Isotope Effects. The magnitude of the *β*-secondary 2′-^{3}H KIE reports on the geometry of ribose at the transition state and is proportional to the vibrational looseness of the C2′−H2′ *σ* bond. Hyperconjugative transfer of electrons from the C2′−H2′ *σ* bond to the partially empty $2p_z$ orbital of C1′ is responsible for these bond changes (*42*). Two factors influence the interaction: (1) the degree of overlap of the C2′−H2′ *σ* bond with the empty $2p_z$ orbital and (2) the $\cos^2\theta$ function of this overlap and the emptiness of $2p_z$ which is proportional to the C1′−N9 bond length. For a completely dissociated ribooxacarbenium ion at the transition state, the maximum 2′-^{3}H KIE of 1.12 was calculated for a $2p_z$−C1′−C2′−H2′ dihedral angle of 0°, and it decreased with the increase in the electron population of the $2p_z$ orbital or the sp^3 character of C1′. The small 1.044 KIE observed for [2′-^{3}H]MTA suggests only modest orbital overlap with $2p_z$ and is similar to that found for human and *P. falciparum* PNPs, 1.031 and 1.036, respectively (Table 3) (*18*). The relatively small 2′-^{3}H KIE indicates that the ribosyl group adopts a 3-endo configuration at the transition state. The transition state of *E. coli* MTAN corresponds to a H1′−C1′−C2′−H2′ dihedral angle of 53°, and the sugar has a small 3-endo pucker corresponding to an O4′−C1′−C2′−C3′ dihedral angle of −10°.

Primary 9-^{15}N Isotope Effect. The 9-^{15}N KIE reports on the rehybridization of adenine N9 at the transition state as the result of reduced C1′−N9 bond order. In addition, enzymatic groups that interact with the adenine ring can alter ring conjugative bonding. The maximum theoretical KIE value predicted for full loss of a covalent bond to N9 is 1.04. The intrinsic KIE of 1.018 suggests significant loss of bond order to N9 at the transition state combined with altered bond conjugation. The computational model of the transition state that best matches the full family of KIEs gives a calculated 9-^{15}N KIE of 1.021, which is within the error limit of the experimental value (Table 4). A natural bond order analysis of the transition state and the substrate indicates that the N9 is $sp^{1.89}$-hybridized at the transition state compared to $sp^{2.29}$

Table 4: Isotope Effects for the Transition State of *E. coli* MTAN Calculated at the B3LYP/6-31G(d,p) Level and Comparison to the Intrinsic KIE at pH 8.5

position	type of KIE	intrinsic KIE	calculated KIE
1′-^{14}C	primary	1.004	1.004
2′-^{3}H	β-secondary	1.044	1.043
9-^{15}N	primary	1.018	1.021
1′-^{3}H	α-secondary	1.160	1.38
4′-^{3}H	γ-secondary	1.015	0.956
5′-^{3}H$_2$	δ-secondary	1.010	1.01 (*pro-R*) 0.99 (*pro-S*)
Me-^{3}H$_3$	remote	1.051	1.069

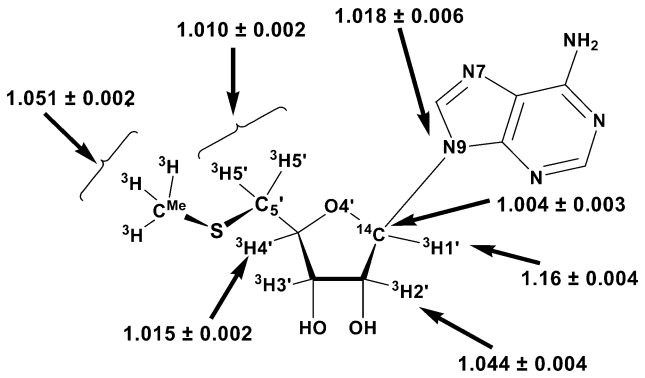

FIGURE 4: Intrinsic kinetic isotope effects measured for the hydrolysis of MTA by *E. coli* MTAN. The KIE for [5′-^{14}C]MTA was assumed to be unity and was used as a control for all the other KIE experiments.

in the substrate; therefore, significant rehybridization occurs at the transition state. The crystal structure of *E. coli* MTAN in complex with a transition state analogue shows that the Oδ2 atom of Asp197 and main chain carbonyl oxygen of Ile152 are hydrogen bonded to N7 and N6 of adenine, respectively (*32*). The H-bonding of N7 to Asp197 is favored by an increased pK_a of N7 at the transition state due to flow of electrons from the ribosyl group into adenine following the cleavage of the N-glycosidic bond. The N7-protonated (neutral) adenine at the transition state forms a better leaving group than adenine anion, facilitating glycosidic bond cleavage. These interactions alter the conjugative system of the adenine ring and influence the hybridization of N9 and the 9-^{15}N KIE.

Remote 4′-^{3}H KIE. The C4′−H4′ σ bond is three bonds from the reaction center, and it was expected that substitution of hydrogen with tritium at this position would not give a significant KIE. A modest KIE of 1.015 was measured experimentally for 4′-^{3}H MTA. However, the computed transition state that best matched the other KIEs predicted a large inverse isotope effect of 0.957 for 4′-^{3}H MTA. Analysis of the natural bond orbitals of the substrate and transition state predicted a large electron delocalization energy (6.59 kcal/mol) in the substrate for hyperconjugation from the lone pair (n_p) of O4′ to the C4′−H4′ antibonding orbital. No hyperconjugation was observed in the transition state for this interaction (<0.5 kcal/mol). Greater hyperconjugation between n_p of O4′ and σ* of the C4′−H4′ group in the substrate relative to the transition state is translated into vibrational looseness to the C4′−H4′ covalent bond in the substrate, giving the inverse calculated KIE in the modeled transition state. At the transition state, the n_p of O4′ is delocalized toward the anomeric carbon both by hyperconjugation to the cationic C1′ and by overlap with the partially empty $2p_z$ orbital of C1′. Calculations on 2-propanol, a secondary alcohol resembling a generic hydroxyl group in ribose, help explain the normal 4′-^{3}H KIE measured with MTAN. Ionization of the 2-propanol hydroxyl gives a large (1.36) isotope effect on the equilibrium of ionization for the central C−H bond (*39*). Hydroxyl deprotonation enhances the ability of oxygen lone pairs to hyperconjugate into the antibonding (σ*) orbital of the geminal CH bond as well as to the vicinal antiperiplanar methyl CH bonds, although to a lesser extent. This lowers the bond order of the geminal CH bond as well as the methyl CH bonds, giving a significant isotope effect on the equilibrium of ionization. The crystal structure of *E. coli* MTAN with MT-ImmA, a transition state analogue inhibitor, shows that the 3′-hydroxyl of ribose forms a 2.7 Å hydrogen bond with Glu174 and a similar H-bond with the catalytic site water (*32*). If hydrogen bonding partially deprotonates the 3′-hydroxyl group at the transition state to moderately increase electron delocalization from n_p of O3′ to σ* of the vicinal C4′−H4′ group, the interaction readily explains the modest KIE of 1.015 at ^{3}H4′ measured experimentally.[5]

5′-^{3}H KIE. No significant KIE is predicated for a position four bonds removed from the site of reaction, and indeed, a modest remote KIE of 1.010 was measured for [5′-^{3}H]MTA. The magnitude of the 5′-^{3}H KIE for *E. coli* MTAN is small compared to that of the KIE of some *N*-ribosyltransferases such as purine nucleoside phosphorylase and thymidine phosphorylase (Table 3). For human and *P. falciparum* PNP, the intrinsic KIEs for [5′-^{3}H]inosine were 1.062 and 1.064 (*18*), respectively, whereas for thymidine phosphorylase, it was 1.061 for [5′-^{3}H]thymidine (*20*). In thymidine phosphorylase, the entire 5′-^{3}H isotope effect is at the step of substrate binding and is due to dihedral freezing of the 5′-hydroxyl (*43*). For PNPs with S_N1 transition states similar to *E. coli* MTAN, it is proposed that hydrogen bonding of the 5′-hydroxyl to histidine in the active site distorts the geometry of 5′-hydrogens at the transition state relative to the ground state, giving rise to the observed KIE (*18*). A 5′-methylthio group of MTA is different from the hydroxymethyl of inosine in hydrophobicity and lack of hydrogen bond potential. The 5′-^{3}H$_2$ KIE (the product of 5′-*pro-R* and 5′-*pro-S* hydrogen isotope effects) of 1.00 was computed using density functional methods [B3LYP/6-31G(d,p)]. The 5′-*pro-R* and 5′-*pro-S* hydrogens behave differently to give isotope effects of 1.010 and 0.99, respectively. The normal isotope effect for the 5′-*pro-R* hydrogen is due to hyperconjugation between the lone pair of sulfur and its antibonding σ orbital. For the 5′-*pro-S* hydrogen, the calculated inverse isotope effect is due to hyperconjugation from the σ bond of the C5′ 5′-*pro-S* hydrogen to the antibonding orbital of the C4′−C5′ group. KIE by definition refers to changes between the reactant and transition state. Conformational freedom of the substrate in solution leads to cancellation of hyperconjugations due to averaging, whereas the 5′ region at the transition state is

[5] Additional evidence for the importance of this 3′-OH interaction comes from the observation that 2′-deoxy-MTA is a good substrate, but 3′-deoxy-MTA is not (*49*), and that a Glu174Ala mutation abolishes catalytic activity (J. E. Lee, W. Luong, D. J. T. Huang, K. A. Cornell, M. K. Riscoe, and P. L. Howell, unpublished observations).

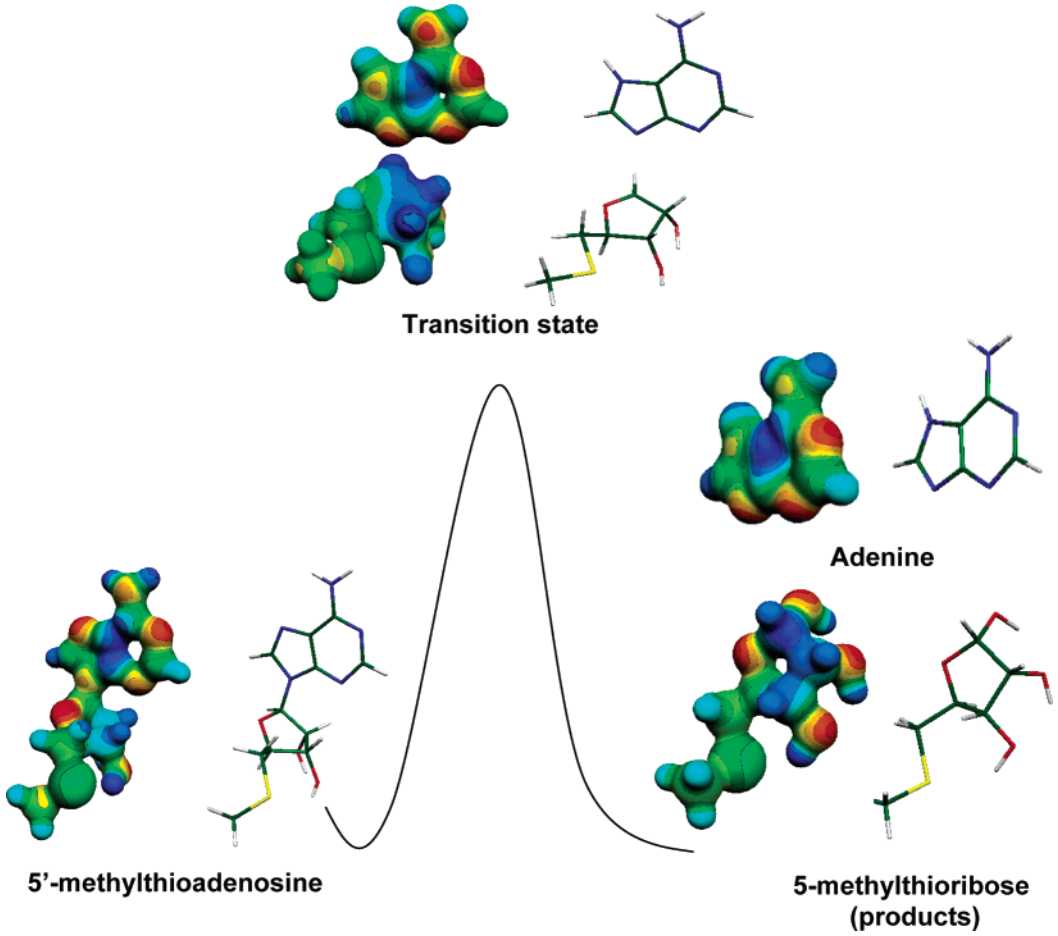

FIGURE 5: Reaction coordinate showing the molecular electrostatic surface potential of 5′-methylthioadenosine (a substrate), the transition state, and adenine with 5-methylthioribose (products). MEPs were calculated at HF/STO3G (*Gaussian98*/cube) for the geometry optimized at the B3LYP/6-31G(d,p) level of theory and visualized with Molekel 4.0 (*34*) at a density of 0.008 electron/b. The stick models shown to the right have the same geometry as the MEP surfaces.

immobile for the short time span of the transition state. Dihedral freezing upon binding and during the transition state coupled with hyperconjugation effects described above is sufficient to explain the observed 5′-^{3}H KIE.

Remote Me-$^3H_3$ KIEs. The methylthio group of 5′-methylthioadenosine is fixed in the active site of *E. coli* MTAN by hydrophobic interaction with nonpolar residues, including Met9, Ile50, Val102, Phe105, and Phe207 (*32*). In solution, MTA will sample all C4′−C5′−S−C^{Me} dihedral angle conformations since calculations suggest that the energetic barrier for full rotation of the C4′−C5′−S−C^{Me} angle is less than 0.7 kcal/mol. An isotope effect of 1.051 was measured for [methyl-$^3H_3$]MTA. C−H bonds of the methyl group are six bonds removed from the *N*-ribosidic bond, and a KIE at this position would be dictated by local effects rather than communication of electron structure from the transition state. The methyl isotope effect is likely to be an equilibrium isotope effect from binding of MTA to the enzyme and the subsequent restriction of C4′−C5′−S−C^{Me} dihedral angle rotation and alteration of C−H vibrational modes. The thiol of the methylthio group contains lone pair electrons. When a C−H bond is adjacent to a heteroatom with a lone pair, hyperconjugation with the antibonding orbital of the C−H bond can decrease its bond order to give a normal isotope effect, depending on the angle by which the C−H bond subtends the lone pair electrons (*38*, *40*). A natural bond orbital analysis of the transition state with fixed methyl group geometry suggests that the n_p of sulfur hyperconjugates with the antibonding orbitals of three methyl C−H bonds with the stabilization energies of 3.98, 4.00, and 1.03 kcal/mol, depending on the C−H bond angles with respect to the lone pair on sulfur. The isotope effects calculated for three methyl C−H bonds are 1.021, 1.031, and 1.016, respectively, to give a predicted isotope effect of 1.069, similar to the isotope effect measured experimentally. The small difference in the calculated KIE can easily arise from uncertainty in accurately predicting the solution and enzymatic conformations of the methylthio group.

Molecular Electrostatic Potential Surface Analysis. The electrostatic potential surface of a molecule is the difference in the interaction energy of a point probe of unit charge between the nucleus and the electrons at a defined distance from the nucleus and, therefore, is sensitive to the distribution of electrons on a molecule (*35*). The electrostatic potential of a substrate changes as it moves along the reaction coordinate, and each position on the reaction coordinate has its own characteristic distribution of electrons and thus a unique molecular electrostatic potential surface (MEP). The MEP surface is a defining attribute of the transition state along with bond distances and charges. The change in MEPs for the substrate, transition state, and products reveals that the leaving group has a higher electron density at the transition state and in the product than the substrate due to flow of electrons from ribose during the conversion of the

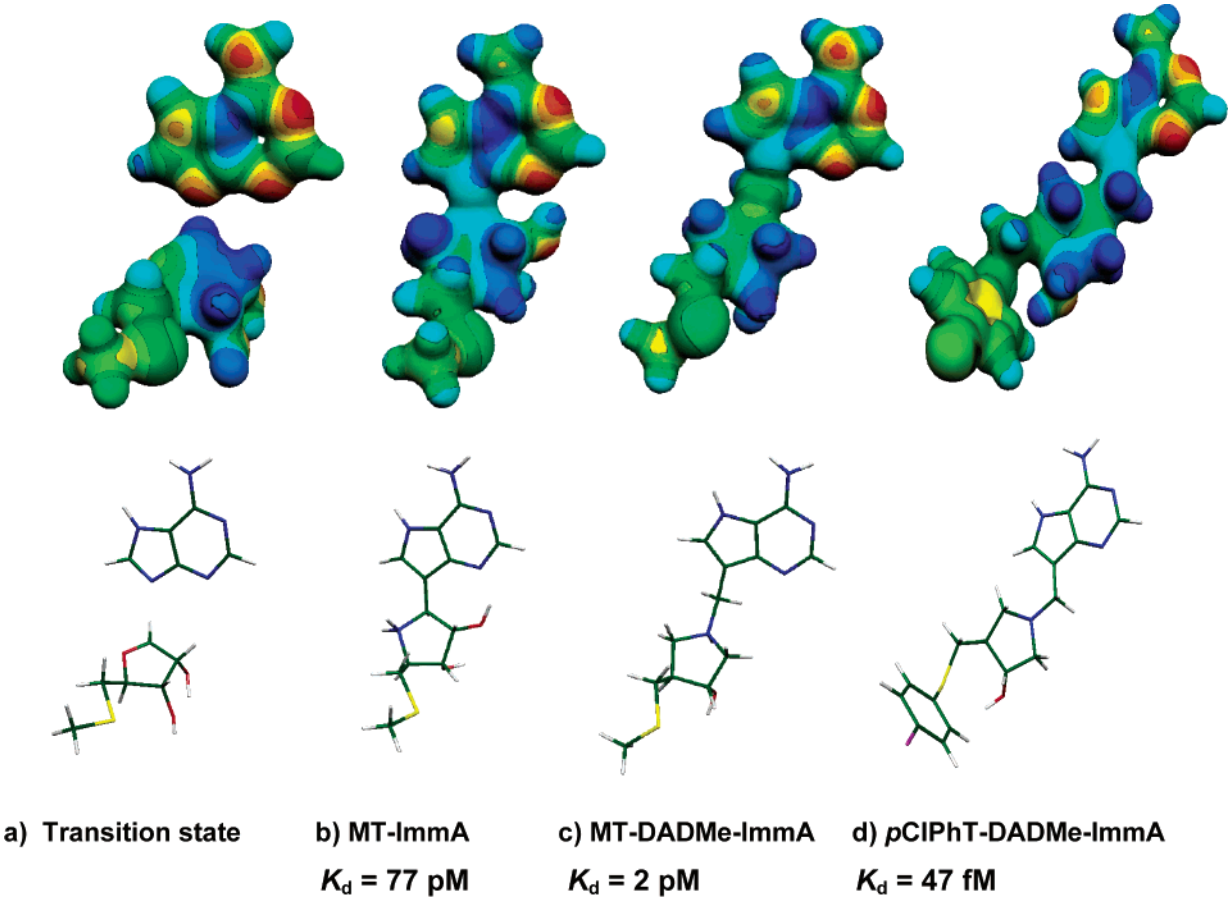

FIGURE 6: Comparison of molecular electrostatic potential surfaces (MEPs) for (a) the transition state of *E. coli* MTAN, (b) MT-ImmA, a 77 pM transition state analogue, (c) MT-DADMe-ImmA, a 2 pM transition state analogue, and (d) *p*ClPhT-DADMe-ImmA, a 47 fM transition state analogue. MEPs were calculated at HF/STO3G (*Gaussian98*/cube) for the optimized geometry at the B3LYP/6-31G(d,p) level of theory and visualized with Molekel 4.0 (*34*) at a density of 0.008 electron/b. The models shown below have the same geometry as the MEP surfaces. The values of K_d are dissociation constants for the inhibitors following slow-onset inhibition or K_i* in slow-onset analysis (*23*).

substrate to the transition state or products, as expected for S_N1 reactions (Figure 5).

Stable Transition State Analogues of the Dissociative Oxacarbenium Ion Transition State of E. coli MTAN. At the transition state of MTAN, the C1′−N9 glycosidic bond of MTA is 3.0 Å long, a loss of 0.96 of the bond order relative to reactant (Table 2). This imparts an increased cationic character to C1′ (the net charge on C1′ increases from 0.25 to 0.50) and increased delocalization of electrons from the lone pairs of the ring oxygen toward the reaction center. The charge on O4′ increases from −0.59 in the reactant to −0.39 at the transition state. The O4′−C1′ bond thus has partial double bond character, and C1′ becomes more planar. Dissociation of the glycosidic bond at the transition state causes an increased pK_a of N7, and N7 is protonated at the transition state to form a favorable hydrogen bond with Asp197. The transition state analogue inhibitors were designed to contain a cationic ribosyl analogue and an elevated pK_a at N7. Replacing N9 of adenine with carbon (9-deazaadenine) creates a stable C−C glycosidic bond and alters the conjugative pattern to increase the pK_a of N7 to >10 (*44*).[2] The MEP surface of the transition state is similar to that of the inhibitors. MT-ImmA, MT-DADMe-ImmA, and *p*ClPhT-DADMe-ImmA are all similar to the transition state (Figure 6). The binding affinity of transition state analogue inhibitors is related to how closely their electrostatics matches that of the transition state. The MEPs of MT-DADMe-ImmA and *p*ClPhT-DADMe-ImmA are better matches to the MEP of the transition state than that of MT-ImmA, consistent with their increased binding affinity for *E. coli* MTAN (Figure 6 and ref *23*).

The first generation of transition state analogue inhibitors, Immucillins, incorporated the features of early ribooxacarbenium ion transition states. N4′ in Immucillins has as a pK_a of 6.9 and is known to be cationic at the catalytic sites of *N*-ribosyltransferases (*44*). Methylthio-Immucillin-A in the Immucillin series resembles MTA at an early transition state. It is a tight-binding slow-onset inhibitor with an overall dissociation constant of 77 pM. The second-generation transition state analogue inhibitors "DADMe-Immucillins" were designed to match the geometry and molecular electrostatic features of fully dissociated ribooxacarbenium ion transition states (*22*). They include a pyrrolidine moiety as the ribooxacarbenium mimic and a methylene bridge between the ribooxacarebenium ion mimic and the 9-deazaadenine to provide geometric approximation for the fully dissociative transition state of *E. coli* MTAN. MT-DADMe-ImmA is a transition state mimic because it incorporates the methylthio group, the cationic mimic of the ribooxacarbenium ion, a methylene bridge to give a 2.5 Å distance to approximate the 3 Å *N*-ribosidic bond of the transition state, and the elevated pK_a at N7. It is a slow-onset inhibitor with an

equilibrium dissociation constant of 2 pM (Figure 6). The tightest inhibitor in the DADMe-Immucillin-A series was *p*ClPhT-DADMe-ImmA. It has a dissociation constant of 47 fM inhibitor and binds 91 million times tighter than the substrate *S*-adenosylhomocysteine ($K_m = 4.3\ \mu M$) and is one of the most powerful noncovalent inhibitors ever reported (*23*). The binding affinity of *p*ClPhT-DADMe-ImmA is within a factor of 1000 of the predicted binding affinity of the transition state calculated on the basis of the k_{cat} of the enzyme relative to chemical solvolysis.

Binding of Femtomolar Transition State Analogue Inhibitors. Defining features of the transition state include the cationic character of the sugar, the increased pK_a of N7, and the 3 Å distance between the ribooxacarbenium ion and N9 of adenine. Although the 4′-iminoribitol group of MT-ImmA is cationic (p$K_a = 6.9$) to mimic the ribooxycarbenium ion nature of the transition state, the C1′−C9 distance is only 1.5 Å in MT-ImmA, short of the 3 Å C1′−N9 bond in the transition state. In the crystal structure, the protonated 4′-iminoribitol group of MT-ImmA can be seen to attract the nucleophilic water toward the 4′-iminoribitol group (∼3.1 Å). In structures with neutral substrate analogues of MTA, such as methylthiotubercidin (7-deaza-MTA), the O4′ ribosyl atom does not interact with the nucleophilic water, and is separated by ∼3.6 Å in the crystal structure (*45*). It has been proposed that the nucleophilic water is deprotonated at the active site to form a strong electrostatic ion pair interaction with the cationic 4′-iminoribitol group. For DADMe-Immucillins, the same features of the transition state account for their tight binding but they are better geometric and electrostatic mimics. The pK_a of the 1′-pyrrolidine nitrogen is ∼8.5 in similar compounds, and they are therefore cationic at neutral pH (*46*). The presence of the cationic N1′ atom and the deletion of the O2′ hydroxyl allow a better capture of the transition state features by allowing the nucleophilic water to move to within ∼2.6 Å of the 1′-pyrrolidine nitrogen. The stronger electrostatic interaction between the pyrrolidine cation and the water nucleophile is proposed to be an important feature for action as transition state mimics (*32*).

CONCLUSION

Kinetic isotope effects and density functional calculations establish the transition state of *E. coli* MTAN to be highly dissociative with very low bond order to the leaving group and no significant bond order to the attacking water nucleophile and the ribosyl moiety to have significant oxacarbenium ion character. Transition state models and natural bond orbital analysis provide explanations for remote isotope effects, more than three bonds from the site of chemistry. The transition state structure obtained here provides a blueprint for the design of powerful transition state analogue inhibitors for *E. coli* MTAN. Molecular electrostatic potential maps of the transition state structure are compared to those for transition state analogue inhibitors. Increasing similarity between the experimentally determined transition state structure and inhibitors causes increased binding affinity. Understanding the transition state structure of *E. coli* MTAN provides additional support to the hypothesis that knowledge of transition state chemistry can be readily applied to the design of powerful transition state analogue inhibitors.

ACKNOWLEDGMENT

We thank Prof. F. Weinhold of the Theoretical Chemistry Institute, University of Wisconsin, Madison, WI, for discussions on natural bond orbital analysis.

REFERENCES

1. Hibasami, H., Borchardt, R. T., Chen, S. Y., Coward, J. K., and Pegg, A. E. (1980) Studies of inhibition of rat spermidine synthase and spermine synthase, *Biochem. J. 187*, 419−428.
2. Carteni-Farina, M., Porcelli, M., Cacciapuoti, G., Zappia, V., Grieko, M., and Difiore, P. P. (1983) *Adv. Polyamine Res. 4*, 779−792.
3. Winzer, K., Hardie, K. R., Burgess, N., Doherty, N., Kirke, D., Holden, M. T., Linforth, R., Cornell, K. A., Taylor, A. J., Hill, P. J., and Williams, P. (2002) LuxS: Its role in central metabolism and the in vitro synthesis of 4-hydroxy-5-methyl-3(2*H*)-furanone, *Microbiology 148*, 909−922.
4. Chen, X., Schauder, S., Potier, N., Dorsselaer, V. A., Pelczer, I., Bassler, B. L., and Hughson, F. M. (2002) Structural identification of a bacterial quorum-sensing signal containing boron, *Nature 415*, 545−549.
5. Williams-Ashman, H. G., Seidenfeld, J., and Galletti, P. (1982) Trends in the biochemical pharmacology of 5′-deoxy-5′-methylthioadenosine, *Biochem. Pharmacol. 31*, 277−288.
6. Miller, M. B., and Bassler, B. L. (2001) Quorum sensing in bacteria, *Annu. Rev. Microbiol. 55*, 165−199.
7. Miller, M. B., Skorupski, K., Lenz, D. H., Taylor, R. K., and Bassler, B. L. (2002) Parallel quorum sensing systems converge to regulate virulence in *Vibrio cholerae*, *Cell 110*, 303−314.
8. Myers, R. W., and Abeles, R. H. (1989) Conversion of 5-*S*-ethyl-5-thio-D-ribose to ethionine in *Klebsiella pneumoniae*. Basis for the selective toxicity of 5-*S*-ethyl-5-thio-D-ribose, *J. Biol. Chem. 264*, 10547−10551.
9. Pegg, A. E. (1983) Inhibition of Aminopropyltransferases. *Methods Enzymol. 94*, 294−297.
10. Pajula, R. L., and Raina, A. (1979) Purification of spermine synthase from bovine brain by spermine-Sepharose affinity chromatography. *FEBS Lett. 99*, 153−156.
11. Parsek, M. R., Val, D. L., Hanzelka, B. L., Cronan, J. E., Jr., and Greenberg, E. P. (1999) Acyl homoserine-lactone quorum-sensing signal generation, *Proc. Natl. Acad. Sci. U.S.A. 96*, 4360−4365.
12. Schauder, S., Shokat, K., Surette, M. G., and Bassler, B. L. (2001) The LuxS family of bacterial autoinducers: Biosynthesis of a novel quorum-sensing signal molecule, *Mol. Microbiol. 41*, 463−476.
13. Wolfenden, R. (1969) Transition state analogues for enzyme catalysis. *Nature 223*, 704−705.
14. Wolfenden, R., and Snider, M. J. (2001) The depth of chemical time and the power of enzymes as catalysts, *Acc. Chem. Res. 34*, 938−945.
15. DeWolf, W. E., Jr., Fullin, F. A., and Schramm, V. L. (1979) The catalytic site of AMP nucleosidase. Substrate specificity and pH effects with AMP and formycin 5′-PO_4, *J. Biol. Chem. 254*, 10868−10875.
16. Horenstein, B. A., and Schramm, V. L. (1993) Correlation of the molecular electrostatic potential surface of an enzymatic transition state with novel transition-state inhibitors, *Biochemistry 32*, 9917−9925.
17. Cornell, K. A., Swarts, W. E., Barry, R. D., and Riscoe, M. K. (1996) Characterization of recombinant *Eschericha coli* 5′-methylthioadenosine/*S*-adenosylhomocysteine nucleosidase: Analysis of enzymatic activity and substrate specificity, *Biochem. Biophys. Res. Commun. 228*, 724−732.
18. Lewandowicz, A., and Schramm, V. L. (2004) Transition state analysis for human and *Plasmodium falciparum* purine nucleoside phosphorylases, *Biochemistry 43*, 1458−1468.
19. Chen, X. Y., Berti, P. J., and Schramm, V. L. (2000) Ricin A-Chain: Kinetic Isotope Effects and Transition State Structures with Stem-Loop RNA, *J. Am. Chem. Soc. 122*, 1609−1617.
20. Birck, M., and Schramm, V. L. (2004) Nucleophilic participation in the transition state for human thymidine phosphorylase, *J. Am. Chem. Soc. 126*, 2447−2453.
21. Schramm, V. L. (2005) Enzymatic transition states: Thermodynamics, dynamics and analogue design. *Arch. Biochem. Biophys. 433*, 13−26.

22. Lewandowicz, A., Tyler, P. C., Evans, G. B., Furneaux, R. H., and Schramm, V. L. (2003) Achieving the ultimate physiological goal in transition state analogue inhibitors for purine nucleoside phosphorylase, *J. Biol. Chem. 278*, 31465−31468.
23. Singh, V., Evans, G. B., Lenz, D. H., Mason, J. M., Clinch, K., Mee, S., Painter, G. F., Tyler, P. C., Furneaux, R. H., Lee, J. E., Howell, P. L., and Schramm, V. L. (2005) Femtomolar transition state analogue inhibitors of 5′-methylthioadenosine/S-adenosylhomocysteine nucleosidase from *Escherichia coli*, *J. Biol. Chem. 280*, 18265−18273.
24. Lee, J. E., Cornell, K. A., Riscoe, M. K., and Howell, P. L. (2001) Expression, purification, crystallization and preliminary X-ray analysis of *Escherichia coli* 5′-methylthioadenosine/S-adenosylhomocysteine nucleosidase, *Acta Crystallogr. D57*, 150−152.
25. Shi, W., Tanaka, K. S. E., Crother, T. R., Taylor, M. W., Almo, S. C., and Schramm, V. L. (2001) Structural analysis of adenine phosphoribosyltransferase from *Saccharomyces cerevisiae*, *Biochemistry 40*, 10800−10809.
26. Parkin, D. W., Leung, H. B., and Schramm, V. L. (1984) Synthesis of nucleotides with specific radiolabels in ribose. Primary ^{14}C and secondary ^{3}H kinetic isotope effects on acid-catalyzed glycosidic bond hydrolysis of AMP, dAMP, and inosine, *J. Biol. Chem. 259*, 9411−9417.
27. Rising, K. A., and Schramm, V. L. (1994) Enzymatic synthesis of NAD^+ with the specific incorporation of atomic labels, *J. Am. Chem. Soc. 116*, 6531−6536.
28. Northrop, D. B. (1975) Steady-state analysis of kinetic isotope effects in enzymic reactions, *Biochemistry 14*, 2644−2651.
29. Rose, I. A. (1980) The isotope trapping method: Desorption rates of productive E.S complexes, *Methods Enzymol. 64*, 47−59.
30. Frisch, M. J., Trucks, G. W., Schlegel, H. B., Scuseria, G. E., Robb, M. A., Cheeseman, J. R., Montgomery, J. A., Jr., Vreven, T., Kudin, K. N., Burant, J. C., Millam, J. M., Iyengar, S. S., Tomasi, J., Barone, V., Mennucci, B., Cossi, M., Scalmani, G., Rega, N., Petersson, G. A., Nakatsuji, H., Hada, M., Ehara, M., Toyota, K., Fukuda, R., Hasegawa, J., Ishida, M., Nakajima, T., Honda, Y., Kitao, O., Nakai, H., Klene, M., Li, X., Knox, J. E., Hratchian, H. P., Cross, J. B., Bakken, V., Adamo, C., Jaramillo, J., Gomperts, R., Stratmann, R. E., Yazyev, O., Austin, A. J., Cammi, R., Pomelli, C., Ochterski, J. W., Ayala, P. Y., Morokuma, K., Voth, G. A., Salvador, P., Dannenberg, J. J., Zakrzewski, V. G., Dapprich, S., Daniels, A. D., Strain, M. C., Farkas, O., Malick, D. K., Rabuck, A. D., Raghavachari, K., Foresman, J. B., Ortiz, J. V., Cui, Q., Baboul, A. G., Clifford, S., Cioslowski, J., Stefanov, B. B., Liu, G., Liashenko, A., Piskorz, P., Komaromi, I., Martin, R. L., Fox, D. J., Keith, T., Al-Laham, M. A., Peng, C. Y., Nanayakkara, A., Challacombe, M., Gill, P. M. W., Johnson, B., Chen, W., Wong, M. W., Gonzalez, C., and Pople, J. A. *Gaussian 03*, revision C.02, Gaussian, Inc., Wallingford, CT.
31. Becke, D. A. (1996) Density-functional thermochemistry. IV. A new dynamical correlation functional and implications for exact-exchange mixing, *J. Chem. Phys. 104*, 1040−1046.
32. Lee, J. E., Singh, V., Evans, G. B., Tyler, P. C., Furneaux, R. H., Cornell, K. A., Riscoe, M. K., Schramm, V. L., and Howell, P. L. (2005) Structural rationale for the affinity of pico- and femtomolar transition state analogues of *E. coli* 5′-methylthioadenosine/S-adenosylhomocysteine nucleosidase, *J. Biol. Chem. 280*, 18274−18282.
33. Anisimov, V., and Paneth, P. (1999) ISOEFF98. A program for studies of isotope effects using Hessian modifications, *J. Math. Chem. 26*, 75−86.
34. Flükiger, P., Lüthi, H. P., Portmann, S., and Weber, J. (2000) *MOLEKEL 4.0*, Swiss Center for Scientific Computing, Manno, Switzerland.
35. Bagdassarian, C. K., Schramm, V. L., and Schwartz, S. D. (1998) Molecular electrostatic potential analysis for enzymatic substrates, competitive inhibitors and transition-state inhibitors, *J. Am. Chem. Soc. 118*, 8825−8836.
36. Berti, P. J., and Tanaka, K. S. E. (2002) Transition state analysis using multiple kinetic isotope effects: Mechanisms of enzymatic and non-enzymatic glycoside hydrolysis and transfer, *Adv. Phys. Org. Chem. 37*, 239−314.
37. Northorp, D. B. (1981) The expression of isotope effects on enzyme-catalyzed reactions, *Annu. Rev. Biochem. 50*, 103−131.
38. Lewis, B. E., and Schramm, V. L. (2001) Conformational equilibrium isotope effects in glucose by ^{13}C NMR spectroscopy and computational studies, *J. Am. Chem. Soc. 123*, 1327−1336
39. Lewis, B. E., and Schramm, V. L. (2003) Isotope effect-mapping of the ionization of glucose demonstrates unusual charge sharing, *J. Am. Chem. Soc. 125*, 7872−7877.
40. Lewis, B. E., and Schramm, V. L. (2003) Binding equilibrium isotope effects for glucose at the catalytic domain of human brain hexokinase, *J. Am. Chem. Soc. 125*, 4785−4798.
41. Pham, T. V., Fang, Y. R., and Westaway, K. C. (1997) Transition state looseness and α-secondary kinetic isotope effects. *J. Am. Chem. Soc. 119*, 227−232.
42. Sunko, D. E., Szele, I., and Hehre, W. J. (1977) Hyperconjugation and the angular dependence of *β*-deuterium isotope effects, *J. Am. Chem. Soc. 99*, 5000−5005.
43. Birck, M. R., and Schramm, V. L. (2004) Binding causes the remote [5′-^{3}H]thymidine kinetic isotope effect in human thymidine phosphorylase, *J. Am. Chem. Soc. 126*, 6882−6883.
44. Sauve, A. A., Cahill, S. M., Zech, S. G., Basso, L. A., Lewandowicz, A., Santos, D. S., Grubenmeyer, C., Evans, G. B., Furneaux, R. H., Basso, L. A., Santos, D. S., Almo, S. C., and Schramm, V. L. (2003) Ionic states of substrates and transition state analogues at the catalytic sites of N-ribosyltransferases, *Biochemistry 42*, 5694−5705.
45. Lee, J. E., Cornell, K. A., Riscoe, M. K., and Howell, P. L. (2003) Structure of *Escherichia coli* 5′-methylthioadenosine/S-adenosylhomocystein nucleosidase inhibitor complexes provide insight into the conformational changes required for substrate binding and catalysis, *J. Biol. Chem. 280*, 8761−8770.
46. Zhou, G. C., Parikh, S. L., Tyler, P. C., Evans, G. B., Furneaux, R. H., Zubkova, O. V., Benjes, P. A., and Schramm, V. L. (2004) Inhibitors of ADP-ribosylating bacterial toxins based on oxacarbenium ion character at their transition states, *J. Am. Chem. Soc. 126*, 5690−5698.
47. Kline, P. C., and Schramm, V. L. (1993) Purine nucleoside phosphorylase. Catalytic mechanism and transition-state analysis of the arsenolysis reaction, *Biochemistry 32*, 13212−13219.
48. Miller, S. T., Xavier, K. B., Campagna, S. R., Taga, M. E., Semmelhack, M. F., Bassler, B. L., and Hughson, F. M. (2004) *Salmonella typhimurium* recognizes a chemically distinct form of the bacterial quorum-sensing signal AI-2, *Mol. Cell 15*, 677−687.
49. Allart, B., Gatel, M., Guillerm, D., and Guillerm, G. (1998) The catalytic mechanism of adenosylhomocysteine/methylthioadenosine nucleosidase from *Escherichia coli*: Chemical evidence for a transition state with a substantial oxocarbenium character, *Eur. J. Biochem. 256*, 155−162.

BI050863A